Plasmonic conversion of solar energy

César Clavero

Plasma Applications Group, Environmental Energy Technologies Division, Lawrence Berkeley National Laboratory, 1 Cyclotron Road, Berkeley, CA, 94720, USA.

Finding new and more efficient paradigms for electron-hole separation is of paramount importance to advance toward a more efficient conversion of solar energy into electricity in photovoltaic cells or into chemical energy in photocatalytic devices. Plasmonic conversion of solar energy has been proposed in recent years as a promising alternative to conventional semiconductor based devices. This novel method is based on the generation of highly energetic electrons, *i.e.* "hot electrons", through electromagnetic decay of surface plasmons in properly designed plasmonic nanostructures. Such "hot electrons" can be extracted from the plasmonic nanostructures and ultimately generate electric currents. Here, the fundamentals of plasmonic energy conversion are reviewed, with special attention to recent progress in the development of this technology toward novel photovoltaic devices. This new way of energy conversion offers interesting possibilities, mainly due to the outstanding light trapping, electromagnetic field concentration and "hot electron" generation properties of surface plasmons. However, several considerations regarding the materials, architectures and fabrication methods used in these kinds of devices need to be carefully regarded to move the field of plasmonic conversion of solar energy forward.

Table of Contents

1. Introduction

The outstanding light trapping and electromagnetic field concentration properties of surface plasmons open up a wide spectrum of applications in the field of Photonics. In essence, surface plasmons are highly confined and intense electromagnetic waves that propagate on the surface of conducting materials due to the interaction of light with the conduction electrons[1], allowing unprecedented control of light in the nanoscale, well below the diffraction limit[1-4]. The novel discipline known as "Plasmonics" has attracted the attention of scientists from very different backgrounds[5], mainly due to the broad range of applications that the use of surface plasmons offer, including miniaturized photonic circuits with length scales much smaller than those currently achieved[6, 7], extreme concentration of light and electromagnetic fields in properly designed nanostructures[2, 4, 8], and remarkably enhanced sensitivity in biosensors[9]. However, in the last few years researchers have also turned their attention to Plasmonics to solve one of the most relevant scientific and technological challenges facing humanity in the 21st century, *i.e.* efficient and affordable generation of clean, abundant energy from renewable energy sources such as the Sun. Indeed, sunlight is by far the most prominent source of clean energy on the surface of Earth, providing enough energy in about one hour to cover the energy demand of the planet in one year[10]. Achieving more efficient energy conversion will allow us to guarantee energy and environmental sustainability within the upcoming decades.

In this scope, recent studies have proposed to use the outstanding light trapping and electromagnetic energy concentration properties of plasmonic nanostructures in combination with conventional semiconductor-based photovoltaic cells and catalytic devices to increase their efficiency[11-15]. However, recent investigations have shown that plasmonic nanostructures can convert the collected light into electric energy by generating electron-hole pairs, also known as excitons[16-18]. After light absorption and surface plasmon excitation in the nanostructures, plasmons can decay transferring the accumulated energy to electrons in the conduction band of the material. This process gives rise to highly energetic electrons, also known as "hot electrons", that can escape the plasmonic nanostructures and be collected by, for example, putting the plasmonic nanostructures in contact with a semiconductor forming a metal-semiconductor Schottky junction[18]. This new paradigm of solar energy

conversion, based on the generation of "hot electrons" through surface plasmon decay, opens a new venue for photovoltaic and photocatalytic devices that can potentially push further the current efficiency limits of conventional devices while lowering the fabrication costs. Nevertheless, some difficulties and limitations inherent to the nature of this energy conversion process, and to the properties of the materials employed, need to be addressed in order to achieve larger efficiencies.

Several reviews have been recently published focusing on the application of plasmonic nanostructures in photocatalytic devices[14, 19-21], mainly due to their outstanding applications for water splitting. The main advantage of these plasmonic photocatalytic systems is the fact that they are able to use the visible region of the spectrum, considerably more abundant on the surface of Earth, and not only ultra violet radiation as it is the case of conventional devices. While encouraging works have been recently published on this field, solar energy conversion aimed at photovoltaic applications is still in its infancy. New approaches and architectures need to be overtaken in order to optimize the "hot electron" generation, injection and regeneration processes in order to obtain efficiencies comparable to state-of-the-art semiconductor based devices. This review is focused on the physical fundamentals of plasmonic energy conversion, with special emphasis in photovoltaic applications. To provide contextual background to this review, we begin with a brief description of the state-of-the-art in solar energy conversion, followed by a detailed description of the fundamentals of plasmonic energy conversion. This is followed by a detailed review of the most significant advances in this field over the last few years. We finish by discussing the directions that should be taken in order to push further the efficiency of this novel energy conversion method, with special attention to the materials, architectures and fabrication methods that could be employed.

2. State-of-the-art in solar energy conversion

As previously mentioned, solar energy can be directly converted into electricity by means of photovoltaic cells, or transformed into chemical energy as in the case of catalytic devices. In the last decades, significant advances have been made to increase the efficiency and lower the cost of solar energy transformation processes. Today's most commonly used solar cells are based on thin film semiconductor architectures, in which photons are captured and generate electron-hole pairs, under the influence of electric fields within the semiconductor[22] [Figure 1 (a)]. While the average efficiencies for solar cells in the market are around 10-15%, record efficiencies of 28.3% have been recently achieved in single junction solar cells[23]. Multi-junction solar cells have considerably broadened the absorption spectrum by combining semiconductors with different band gaps, recently achieving record efficiencies up to 43.5%[23]. Nevertheless, concentrated illumination of 400-600 suns is necessary to reach such high efficiency values[24].

The efficiency of semiconductor based solar cells is limited by some fundamental factors directly related to their own nature and the exciton generation process[25]. Carrier thermalization and inefficient light absorption are the most important sources of thermodynamic losses in conventional solar-energy conversion systems, accounting for more than a 40 % of the total loss in efficiency[25]. As it is illustrated in Figure 1 (b), only photons with energies ($\hbar\omega$) higher than the band-gap of the semiconductor E_g can be absorbed in these solar cells. An electron-hole pair is formed across the band gap with energy E_g after thermalization in the conduction band. The

difference between the absorbed photon energy and the band gap is lost to heat. Photons with energies lower than the band gap energy E_g cannot be absorbed and their energy is also lost. In addition to such thermodynamic limitations, a considerable part of the losses are due to incomplete light trapping by the solar cells[13]. Current crystalline Si semiconductor devices need to be in the 180-300 µm thickness range due to the low absorption cross section of Si, which accounts for most of the cost of the cells. It is highly desirable to obtain thinner architectures (in the 1 to 2 µm range) on inexpensive substrates[13]. Other factors such as overheating, considerably decrease the efficiency of these kinds of devices, and make refrigeration necessary in the case of concentrated photovoltaics.

Second generation photovoltaic devices consist of thin-film cells made out of amorphous silicon, CdTe or copper indium gallium diselenide (CIGS). Third generation devices are based on cells made from inexpensive oxide semiconductor materials coated with light sensitive dyes, photoactive organic polymeric materials, and quantum dots. In most cases, "hot electrons" are generated by means of exothermic chemical processes[26-28,29] [Figure 1 (c)]. However, the performance obtained is unsatisfactory, mainly due to the ineffectiveness of the absorbed dye molecules in producing photocurrents and the recombination of carriers before being injected. These new approaches are far from offering efficiencies high enough to compete with fossil fuels. New paradigms for photon capture and conversion are needed to meet the future goals of energy and environmental sustainability. In this scope, plasmonic electron-hole pair generation and injection is a novel method of solar energy conversion that can lead to unprecedented efficiencies, mainly due to the outstanding light trapping and concentration properties of surface plasmons[11, 13, 15]. The fundamentals of plasmonic energy conversion are reviewed in detail in the following section.

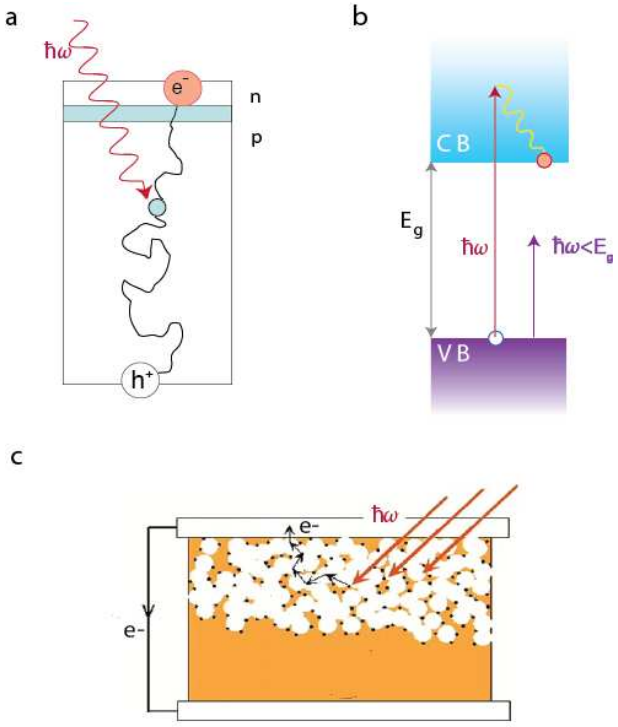

Figure 1 Charge separation in conventional solar cells. (a) In first generation semiconductor solar cells based on semiconductor *p-n* junctions, photons recombine forming electron-hole pairs. (b) Only photons with energies $\hbar\omega$ higher than the band gap E_g can be absorbed. (c) Second generation dye sensitized cells employ dyes to sensitize a cyclic photochemical photovoltaic process that mimics photosynthesis.

3. Plasmonic energy conversion fundamentals

3.1. Surface plasmons

As previously mentioned, surface plasmons are electromagnetic waves that propagate along the surface of materials with free electrons such as metals, conducting oxides and semiconductors, in response to external illumination such as solar radiation[1-3]. They are essentially light waves trapped on the surface because of their interaction with the free electrons of the conductor. Strictly speaking, they should be referred as surface plasmon polaritons (SPPs) to reflect this hybrid nature. The free electrons on the surface respond collectively by oscillating in resonance with the light wave. The resonant interaction between the surface charge oscillation and the electromagnetic field of the light constitutes the SPP, and gives rise to its unique properties. In addition to surface plasmons on flat surfaces, localized surface plasma excitations can appear in nanostructures with confined electrons. Localized Surface Plasmon Resonance[1, 30] (LSPR) can appear in properly designed nanostructures, in which the confined electrons oscillate following the incident radiation frequency and eventually can enter resonance [Figure 2 (a) and (b)]. LSPR resonance takes place in the visible range for the case of metals such as Au and Ag [Figure 2 (c)], while oxides and semiconductors with lower carrier concentrations exhibit resonances in the near infrared and infrared ranges. Propagating surface plasmon polaritons can also appear on flat and corrugated surfaces as two-dimensional electromagnetic waves bonded to the surface that propagate up to several microns on metals such as Au and Ag[8] [Figure 2 (d) and (e)].

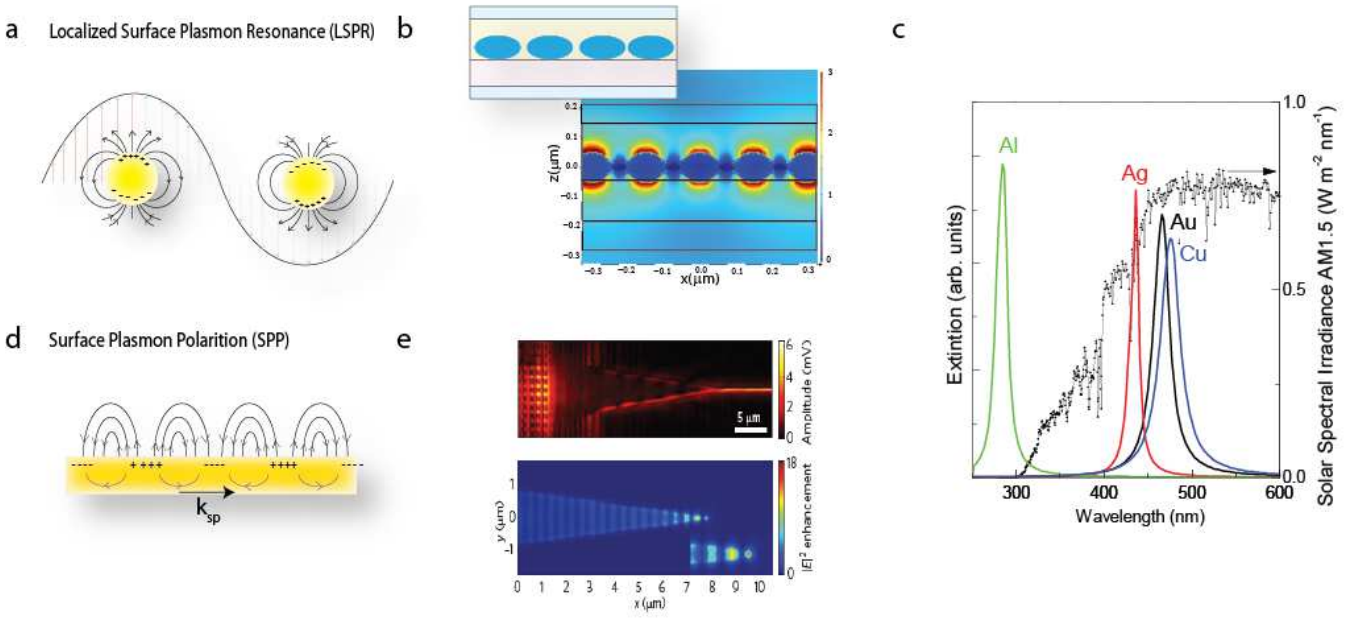

Figure 2 Surface plasmon polariton excitation and absorption. (a) Localized surface plasmon resonance (LSPR) results from the collective oscillation of the electrons confined in a nanostructure in response to external radiation, generating very strong and localized electromagnetic fields as depicted in (b). (c) Optical extinction of Al, Ag, Au and Cu nanoparticles in relation to the solar spectral intensity. (d) Surface plasmon polaritons (SPPs) appear on flat or corrugated surfaces and also give rise to intense electromagnetic fields confined to the surface. (e) NSOM measurements (top) and finite difference time domain simulations (bottom) illustrating SPP focusing using a tapered metal strip waveguide. Figure (e) reproduced with permission of ref. 31, © Optical Society of America 2008.

Surface plasmons impart metal, semiconductor, and conducting oxide nanostructures with high light absorption cross sections and extreme electromagnetic field localization at wavelengths abundant in the solar spectrum. Both of these characteristics are of paramount importance in photovoltaic and photocatalytic devices. Absorption cross sections of plasmonic nanostructures are up to 10^5 larger than typical dye-sensitizer molecules[14, 32]. As such, they have been proposed as efficient light trapping components integrated in photovoltaic cells[12, 13], considerably increasing the efficiency of conventional architectures[12, 13]. In addition, use of plasmonic elements can lead to a significant size reduction. Plasmonic based devices are able to achieve efficient light trapping for thicknesses below 1 μm[13], in stark contrast with single crystal Si semiconductor solar cells. In other cases, the remarkable enhancement of the electromagnetic local field generated by surface plasmons has been shown to increase the charge separation process in the neighboring semiconductor[33].

While all these approaches have proven to increase the energy transformation efficiency, a revolutionary new way of using plasmonic nanostructures in photovoltaic and photocatalytic devices based on plasmonic charge separation has been proposed in recent years. After excitation, surface plasmons can decay, transmitting their energy to electrons in the valence band that become highly energetic electrons known as "hot electrons". Such photoexcited electrons can be properly harvested giving rise to photocurrents in the case of photovoltaic devices, or can be used for reduction and oxidation reaction in photocatalysis devices[14, 34, 35]. The fundamentals of "hot electron" generation are described in detail in the following section.

3.2. Plasmonic energy conversion

Electrons not in thermal equilibrium with the atoms in the metal are frequently referred to as "hot electrons"[37]. When illuminated with highly energetic photons, *e.g.* ultraviolet radiation, some of such "hot electrons" can be emitted from matter owing to the well known photoelectric effect[36]. Photoexcited electrons with energies higher than the work function of the material in which they are contained are emitted, ultimately creating a photocurrent. However, the solar spectrum is mostly composed of less energetic photons falling in the visible and near infrared ranges, which makes the use of this effect impractical for photovoltaic devices. "Hot electrons" can also be generated by exothermic chemical processes[26, 27], as those present in dye sensitized solar cells[28]. In these kinds of devices, a dye molecule anchored to a semiconductor absorbs the incoming light and transfers energetic charge carriers to the semiconductor[29] [Figure 1 (c)]. Nevertheless, the efficiency of dye-sensitized solar cells has only reached a record value of 11 % [23], considerably inferior to conventional single junction semiconductor-based solar cells.

Plasmonic nanostructures can act as efficient "hot electron" generators, transforming visible and near-infrared radiation, abundant in the solar spectrum. Following to light absorption and excitation of surface plasmons in the nanostructures, electromagnetic decay takes place on a femtosecond time scale either radiatively as reemitted photons[38], or non-radiatively by transferring their energy to "hot electrons"[39, 40] [Figure 3 (a)]. Through the latter process, surface plasmons decay first into single-electron excited states, which might be followed by photoemission if their energy exceeds the work function of the material[39, 41]. Two photon processes have also been described[42, 43]. The rest of the photoexcited electrons relax through electron-electron and electron-phonon collisions and ultimately are converted into heat. To illustrate this process, Figure 3 (b) depicts the parabolic density of states (DOS) in the conduction band of a plasmonic nanostructure as a function of energy. All the electronic states below the Fermi energy of the metal $E_{F,M}$ are occupied. After non-radiative

surface plasmon decay, electrons from occupied energy levels are excited above the Fermi energy. Conventional surface plasmons in metal nanostructures can transmit energies $\hbar\omega_p$ between 1 and 4 eV to photoexcited electrons depending on the material, where ω_p is the frequency of the surface plasmon resonance. The generated "hot electrons" need to be efficiently extracted from the plasmonic nanostructures creating an electric current in order for this process to be applicable to energy conversion.

An efficient mechanism to capture photoexcited electrons from plasmon decay in metal nanostructures, for example, is by forming a Schottky barrier with an appropriate semiconductor. Figure 3 (b) shows a Schottky barrier between a plasmonic nanostructure and an *n*-type semiconductor such as TiO_2. "Hot electrons" with energies higher than the Schottky barrier energy $\phi_{SB}= \phi_M-\chi_s$ can escape the plasmonic nanostructure, and are injected into the conduction band of the neighboring semiconductor, where ϕ_M is the work function of the metal and χ_s the electron affinity of the semiconductor[44]. In addition, tunneling across the barrier can take place with a much lower probability[45]. The energy needed for the photoexcited electrons to overcome the energy barrier is considerably smaller than the band gap of the semiconductor E_g, which is in stark contrast with conventional semiconductor-based photovoltaic devices. After injection of "hot electrons" into the neighboring semiconductor, the plasmonic nanostructures are left positively charged due to electronic depletion. An electron donor solution, or a hole transporting material (HTM), is required in contact with them to transport the generated holes to the counter electrode, keeping electric balance and sustaining an electric current. As it will be shown, a large number of HTMs supporting different red-ox reactions have been tested so far, yielding different efficiencies depending on the nature of the plasmonic nanostructures.

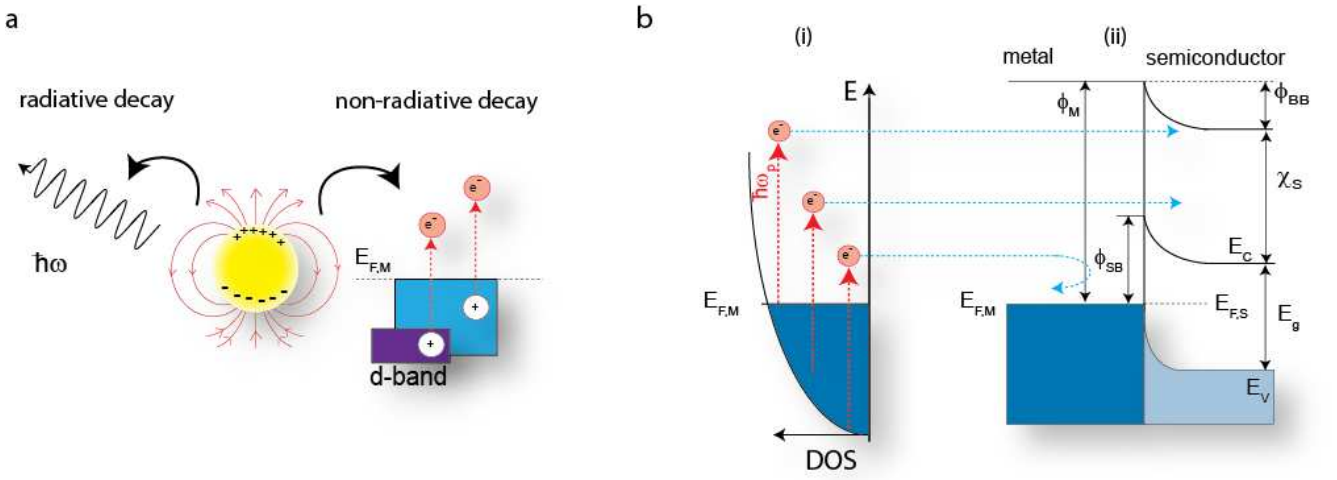

Figure 3 Surface plasmon decay and charge separation. (a) After excitation, surface plasmons can decay radiatively via reemitted photons or non-radiatively via excitation of "hot electrons" within the conduction band or between deeper bands such as the *d* band in the case of noble metals[38] . (b) Plasmonic energy conversion: (i) After non-radiative surface plasmon decay, electrons from occupied energy levels are excited above the Fermi energy. The parabolic density of states (DOS) in the conduction band of the metal is represented as a function of energy. (ii) The plasmonic nanostructures are in contact with a semiconductor forming a Schottky barrier. Hot electrons with energies high enough to overcome the Schottky barrier ϕ_{SB} and are injected into the conduction band E_c of the neighboring semiconductor[44], while those with lower energies are reflected back into the metal.

One of the main advantages of this energy conversion method is the fact that size, shape, and composition of the plasmonic nanostructures can be adapted to obtain a broad absorption across the whole solar spectrum. In addition, the high absorption cross section of plasmonic nanostructures allows decreasing the thickness of the active zone while obtaining a high trapping efficiency. Another important factor that makes plasmonic exciton generation attractive for photovoltaic and photocatalytic devices is that overheating does not negatively affect the exciton generation and injection processes. On the contrary, preliminary studies have shown how their efficiency slightly increases with increased temperature due to increased "hot electron" injection probability[46]. All these points clearly suggest that plasmonic devices are not affected by the same thermodynamic factors that restrain the efficiencies of conventional semiconductor based devices, and therefore open a new horizon of possibilities in the field of solar energy conversion.

4. Advances in Plasmonic energy conversion

4.1. First steps toward plasmonic energy conversion

Early works in 1996 showed hints of surface plasmon induced charge separation in noble metal nanoparticles in contact with semiconductors such as TiO_2. Zhao *et al.*[16] reported for the first time anodic photocurrents in response to visible light in TiO_2 electrodes with a TiO_2 overlayer containing gold or silver metal nanoparticles. This result was striking since photocurrents are only obtained in conventional TiO_2 electrodes when illuminated with ultraviolet light, due to its wide 3.3 eV band gap. While the origin of these photocurrents was unclear at that time, they pointed at the excitation of LSPR in the nanoparticles as a possible mechanism. Indeed, TiO_2 is well known as a good electron-accepting metal oxide due to the high density of states in its conductions band, which allows fast injection of photoexcited electrons.

This research field remained dormant for some years until 2003, when multicolor photochromism, *i.e.* reversible change in color upon illumination, was reported in Ag nanoparticles dispersed in TiO_2. This phenomenon was ascribed to LSPR induced charge separation and oxidation of the Ag nanoparticles[47, 48]. Figure 4 shows such Ag nanoparticles with a broad distribution of sizes, deposited on TiO_2, and illuminated with different wavelengths. When illuminated with a certain wavelength, those nanoparticles undergoing LSPR at such wavelength lose electrons due to charge separation, experience a shift in their plasma resonance, and ultimately lose their ability to absorb that particular wavelength. Since the remaining nanoparticles continue to absorb the rest of the wavelengths, the color of the original excitation wavelength shows up on the film. The inverse process, *i.e.* reversible injection of electrons from TiO_2 into Ag in core-shell Ag-TiO_2 nanoparticles was also demonstrated by Hirakawa *et al.*[49] In their case, the electronic density increase taking place in the Ag core under resonance gives rise to a remarkable shift of the plasmonic absorption from 470 to 430 nm.

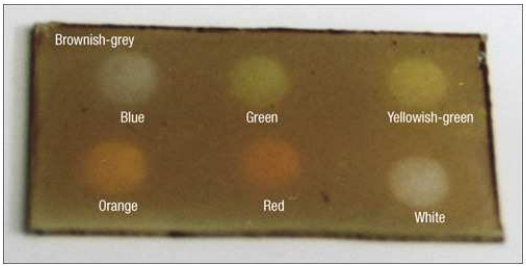

Figure 4. Photochromism in Ag nanoparticles due to charge separation. Ag nanoparticles deposited on TiO_2 exhibit a large diversity of sizes and shapes. A reversible change in color upon illumination is observed due to LSPR induced charge separation and oxidation of the Ag nanoparticles. Figure reproduced with permission of ref. 47. © 2002 Nature Publishing Group.

Shortly after these studies, Tatsuma *et al.*[17, 18, 50-52] demonstrated the three steps required to generate a photoinduced closed circuit current, *i.e.* charge separation, carrier injection and carrier regeneration. In this case, a system consisting of Au or Ag nanoparticles absorbed onto nanoporous TiO_2 and in contact with an electron donor solution was investigated [Figure 5 (a)]. They observed how photoexcited electrons were injected into the TiO_2 matrix upon illumination with visible light and excitation of LSPR in the nanoparticles. They experimentally observed coloring of the TiO_2 substrate under visible light irradiation in open circuit conditions, due to the fact that TiO_2 is a semiconductor whose absorbance in the visible changes when electrons are injected in its conduction band. This clearly demonstrates that electrons are directly injected into the conduction band of the semiconductor after charge separation in the plasmonic nanostructures.

Multiple experiments have been carried out thereafter using this property of TiO_2 to estimate the timescale of the charge separation and injection process, as it will be shown in the following section. Simultaneously, to electron injection, compensative electrons from a donor solution in contact with the plasmonic nanoparticles are injected into them, balancing their electronic deficit and creating an electric circuit [Figure 5 (b)]. Even though the surface plasmon induced charge separation process was still not well understood at that time, the fact that the measured action spectra, *i.e.* incident photon-to-electron conversion efficiency (IPCE) *vs*. wavelength, reproduces exactly the extinction spectra of the Au nanoparticles, clearly indicated that LSPR plays a key role in promoting charge separation [Figure 5 (c)].

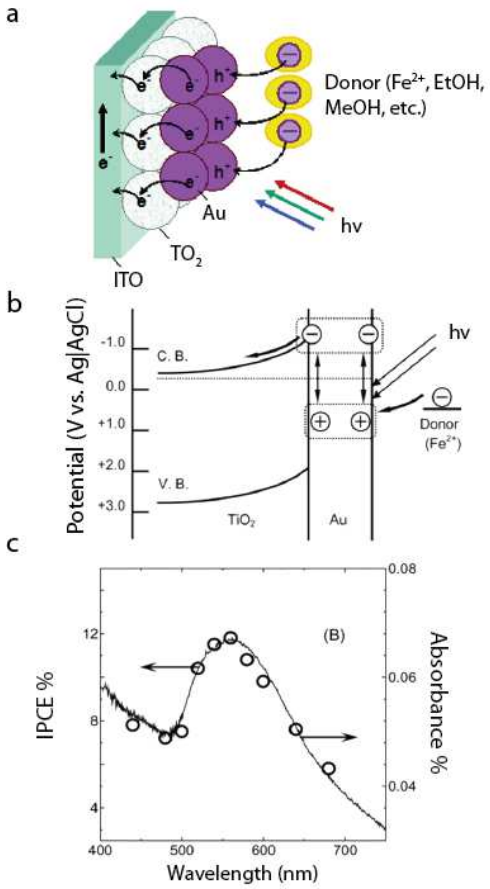

Figure 5 . **Plasmonic charge separation, carrier injection and regeneration**. (a) Sketch of the system proposed by Tatsuma *et al.*[17, 18] consisting of Au nanoparticles deposited on nanoporous TiO_2 and in contact with an electron donor solution. LSPR is excited in the nanoparticles giving rise to charge separation and injection into TiO_2. Simultaneously, electrons from the electron donor solution are injected in the nanoparticles balancing their electronic deficit. (b) Band diagram illustrating the plasmon induced charge separation. (c) The action spectra and extinction spectra share the same spectral shape. Figures reproduced with permission of ref. [18]. © 2005 American Chemical Society.

4.2. Timescale of charge separation, carrier injection and regeneration

Several works have focused on the timescale of the charge separation and injection mechanisms in photoexcited plasmonic nanostructures[52-56]. Fast electron injection in the neighboring semiconductor is a key factor to decrease the recombination of carriers and thus to increase the efficiency of the process. These studies take advantage of the increase of the visible and infrared absorbance of TiO_2 when electrons are injected in its conduction band[18, 52, 53]. Furube *et al.*[53, 55, 56] carried out ultrafast visible-pump/infrared-probe femtosecond transient absorption spectroscopy experiments to characterize the charge transfer kinetics. LSPR was excited in Au nanoparticles deposited on TiO_2 using 150 fs long laser pulses with 550 nm wavelength. Simultaneously, the transient absorption of TiO_2 at 3500 nm was monitored. They found that “hot electron” generation and injection was complete within 50 fs. The timescale of the electron injection found is in agreement with the electron dynamics in the noble metal nanoparticles[57-59]. Relaxation of electrons with a non-Fermi distribution takes place

for times < 100 fs in photoexcited gold nanoparticles. Thus, the electronic injection into the TiO_2 conduction band takes place before or during the electron-electron scattering process[55].

Interestingly, comparison of the Au-TiO_2 response with ruthenium dye N3 (see abbreviations section), known to have a close to 100 % carrier injection efficiency, allowed them to determine an injection efficiency for Au-TiO_2 around 40 % under 550 nm excitation [Figure 6 (a)]. After electron injection, the charge recombination decay was monitored in a longer timescale. Electrons were observed to decay back to the Au nanoparticles after 1.5 ns when no donor solution or HTM layer was in contact with them. Nevertheless, this recombination time depends strongly on the size of the TiO_2 nanoparticles. Tian *et al.*[52, 54], investigated the timescale of the charge regeneration process with different electron donor layers in contact with the Au nanoparticles. They employed, $[Fe(CN)_6]^{4-}$, Fe^{2+}, ferrocenecarboxylic acid[54], and also polyethylene oxide (PEO) filled with TiO_2 nanoparticles[52] as electron donors. After photoexcitation with 5 ns pulses of 532 nm radiation, the transient absorption at 550 nm associated to photoexcited electron injection in TiO_2 was monitored. In the absence of a HTM film, recombination into the Au nanoparticles takes place and is completed after about 200 ns. In contrast, the oxidized Au nanoparticles were shown to be totally regenerated in less than 20 ns in the presence of an electron donor layer.

Finding new ways of faster "hot electron" injection in the semiconductor before loss of energy through electron-electron collisions takes place, and rapid carrier regeneration processes using optimized donor solutions or HTMs, is of paramount importance to maximize the energy conversion efficiency of this process. Several considerations in this sense, regarding the role of the size and shape of the plasmonic nanostructures, semiconductor material employed, and donor solutions or HTM used, are presented in the following sections.

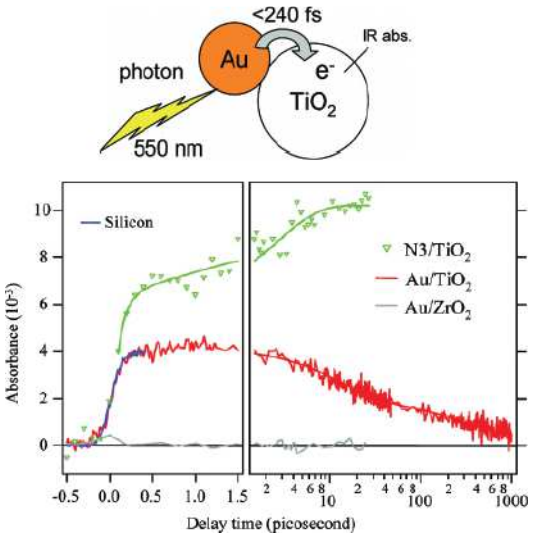

Figure 6. **Timescale of charge separation, carrier injection and regeneration**. Ultrafast visible-pump/IR-probe femtosecond transient absorption spectroscopy shows the timescale of carrier injection in the conduction band of TiO_2. Figures reproduced with permission of ref. 53. © 2007 American Chemical Society.

4.3. Effect of size and shape of the plasmonic nanostructures

Size and shape of the active plasmonic nanostructures are among the most important factors in the processes of surface plasmon excitation and charge separation. They not only affect the wavelength at which LSPR takes place, but also the efficiency of the charge separation process. As previously mentioned, surface plasmons decay by either radiative emission of photons, which is the dominant process in large nanostructures above 20 to 40 nm in the case of Au and Ag[30], or through non-radiative excitation of "hot electrons", as it is the case of smaller nanostructures[14]. The size at which radiative decay starts being the predominant process strongly depends on the optical characteristics of the material. Langhammer *et al.*[60] investigated this dependence in Ag, Pt and Pd nano-discs patterned using lithography of different sizes ranging from 38 to 530 nm. Interestingly, non-radiative decay was found to be the predominant process for Pd and Pt nanodiscs in all the investigated sizes. In contrast, non-radiative scattering was observed to disappear for Ag particle diameters larger than 110 nm. Interestingly, fewer electron-hole pairs are created via LSPR decay in Ag as compared to Pt and Pd despite its higher total extinction. Tatsuma *et al.*[50] investigated the role of size in the charge separation process of Au nanoparticles. They observed larger photocurrents for nanoparticles of 15 nm in diameter as compared with larger ones due to the more efficient decay of surface plasmons into "hot electrons". All these findings emphasize how size and building material of the active plasmonic nanostructures need to be carefully chosen to allow optimum energy conversion.

While spherical nanoparticles exhibit a single plasmon resonance peak, structures such as nano-rods exhibit two characteristic peaks corresponding to the longitudinal and transverse modes. Misawa *et al.*[46, 61, 62] investigated this point in periodically distributed Au rods nanopatterned on *n*-type TiO_2 single crystal substrates [Figure 7 (a)]. The obtained double peak extinction spectra allow extending the range of optical absorption, typically in the visible range for Au, to the near infrared region, covering a considerably larger portion of the solar radiation spectrum [Figure 7 (b)]. The obtained action curves reproduce accurately the extinction spectra of the nanorods [Figure 7 (c)], reaching maximum values of IPCE around 8.4% when immersed in an electrolyte donor solution. Strikingly, the photoelectric conversion efficiency obtained with these plasmonic structures increases with temperature contrary to the general trend in semiconductor based solar cells [Figure 7 (d)]. This remarkable result shows how plasmonic photocurrent generation could solve the problem of overheating in conventional photovoltaic cells. Recently, other works have shown efficient photocatalysis in nanorod based plasmonic systems[63]. Ingram et *al.*[64] showed the role of shape and composition in plasmonic nanostructures by investigating Ag nanocubes and Au nanospheres on TiO_2 and N-TiO_2.

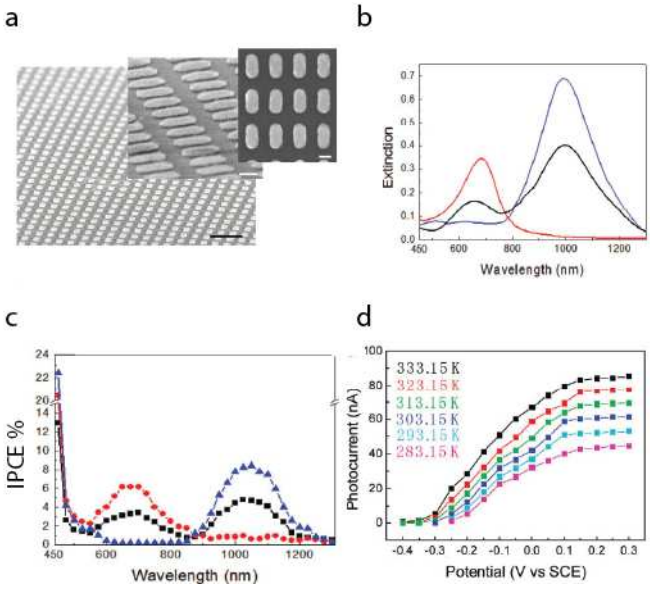

Figure 7. **Plasmonic nanorods.** (a) Scanning transmission microscopy (SEM) images of nanopatterned Au nanorods. (b) Extinction spectra corresponding non-polarized light (black), polarized light along the minor (red) and major (blue) axis direction of the nanorods. (c) The action spectra reproduce the previously observed extinction spectra proving the prominent role of LSPR in this process. (d) A progressive increase of the photocurrent is observed as temperature increases in stark contrast with conventional solar cells. Figures reproduced with permission of ref. 46. © American Chemical Society.

Several works have provided insight into the localization of the charge separation process in plasmonic nanostructures. Tatsuma *et al.* [65, 66] showed how the preferential charge separation sites are those exposed to higher electromagnetic fields in Ag nanorods on TiO_2. After LSPR excitation and charge separation, the oxidized Ag^+ ions diffuse on the water layer adsorbed on the TiO_2 substrate and eventually recombined with electrons from TiO_2 leading to satellite re-deposited islands [Figure 8 (a)]. Such islands appeared in those locations where the LSPR electromagnetic field is more intense. This result confirms the hypothesis that the charge generation process is induced and/or promoted by the intense electromagnetic fields in the plasmonic nanostructures [Figure 8 (b)]. Proper design of the plasmonic nanostructures aimed at maximizing the electromagnetic fields will lead to an increase of this process.

As shown, size and shape of the plasmonic elements are extremely important factors to achieve good energy conversion. Nevertheless, the geometry and relative position of the plasmonic nanostructures with respect to the neighboring semiconductor material are also very important considerations that need to be carefully regarded. Knight *et al.* [67] showed that the photocurrent generated by an active plasmonic element can be significantly enhanced by embedding it in the neighboring semiconductor. This allows for a more efficient transfer of “hot electrons”. In addition, as it will be shown in the following section, direct contact between the donor solution or HTM with the semiconductor material needs to be avoided to preclude detrimental recombination of carriers.

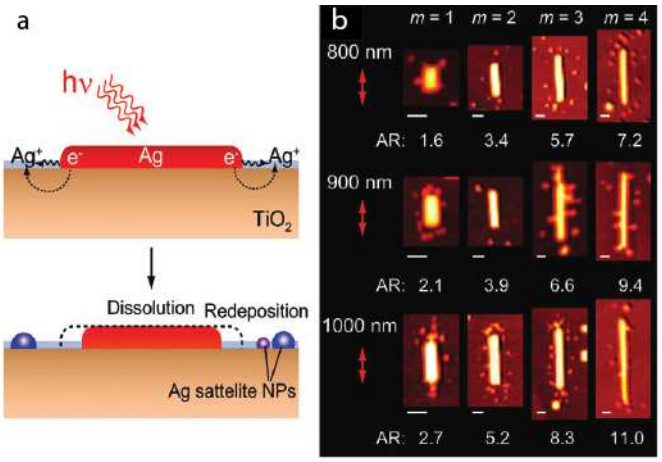

Figure 8. Charge separation localization. (a) Oxidation of Ag nanorods and re-deposition of small Ag nanoparticles takes place due to plasmon-induced charge separation. (b) Tapping-mode AFM images of Ag nanorods after irradiation with 800, 900, and 1000 nm light polarized along the long axis of the nanorods. All scale bars are 50 nm. Figures reproduced with permission from ref. 66 © 2012 ACS.

4.4. Role of the semiconductor electron acceptor material

Following the pioneering studies previously mentioned, a large number of works have been published on charge separation in plasmonic nanostructures aimed at both photovoltaic and catalytic devices. Most of them involve Au or Ag nanoparticles in contact with TiO_2[64, 68-80] [Figure 9 (a)], but more recently other combinations of materials and architectures have been proposed. This is the case of multilayer assemblies of Au nanoparticles and TiO_2 nanosheets[81], Pt nanoparticles on TiO_2 thin films[82], Ag decorated TiO_2 nanotube arrays[78, 83] [Figure 9 (b)], ZnO nanorods decorated with Au nanoparticles[84, 85], hierarchical Au-ZnO flower-rod heterostructures[86] [Figure 9 (c)], Au nanoparticles in contact with CeO_2[87 88], silver halides AgBr decorated with Ag nanoparticles and dispersed in Al_2O_3[89], Ag-AgI supported on mesoporous alumina[90], AgCl particles decorated with Ag nanoparticles[91], core shell SiO_2-TiO_2 nanoparticles decorated with Au nanoparticles[92], M@TiO_2 core-shell nanocomposites (with M = Au, Pd, Pt)[93, 94] [Figure 9 (d)] and Au nanoprisms on WO_2[95]. The choice of an adequate semiconductor to trap the photoexcited "hot electrons" greatly impacts the charge injection mechanisms since it affects the height of the semiconductor-metal Schottky barrier and the number of available states in the conduction band for the incoming electrons. Good alignment of the Fermi level of the plasmonic metal with the band levels of the semiconductor is important to favor efficient charge transfer.[33] In this sense, wide band gap semiconductors have proven to be more efficient capturing "hot electrons". The most relevant example is TiO_2, a wide band gap semiconductor (Eg = 3.3 eV) that has been widely used in plasmonic charge separation due to the high density of states in its conduction band. This fact is mainly due to the *d*-orbital nature of its conduction band, as compared with other typical metal oxides such as ZnO, SnO_2, In_2O_3, whose conduction band is mainly composed of the *s* or *sp* orbital of the metal atoms[55]. In addition, it has no photoresponse in the visible. Other wide band gap semiconductors have been used, such as CeO_2, AgBr, AgI, AgCl and WO_2, as previously shown. Also, recent works have investigated the effect of nanostructuring the semiconducting material. For example, Zhang *et al.* [96] proposed Au nanocrystals assembled on a TiO_2 based photonic crystal. In this case, the matching of the Au nanocrystals LSPR with the photonic crystal photonic band gap significantly increases the LSPR

intensity and boosts the photocatalytic properties. More considerations regarding the semiconductor materials employed, and the matching with the plasmonic nanostructure band will be presented in section 5.3.

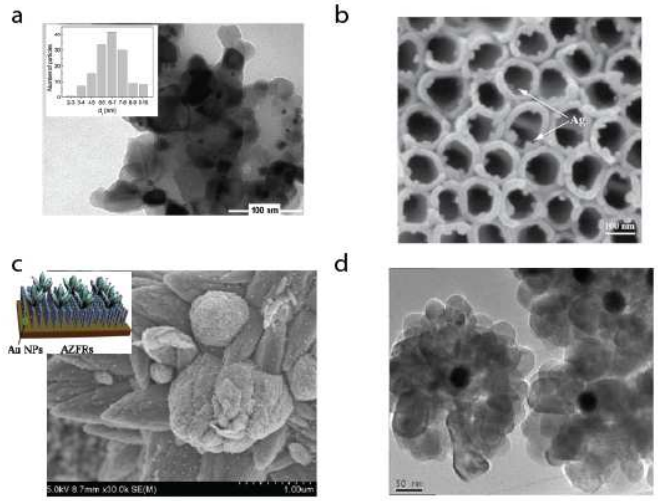

Figure 9 (a) Transmission electron microscopy (TEM) micrographs and particle size distribution of Au/TiO_2[71]. (b) SEM image of Ag on TiO_2 nanotubes[78]. (c) SEM image of Au nanoparticles on oriented hierarchical ZnO flower-rod[86]. (d) TEM images of Au-TiO_2 core-shell nanoparticles[93]. Figures reproduced with permission from: a, b, c, d refs 71, 78, 86, 93 respectively. © 2011 American Chemical Society, © Springer Science+Business Media, LLC 2012, © Springer Science+Business Media New York 2013 and © 2011 American Chemical Society respectively.

4.5. Role of the hole transporting materials

As previously mentioned, the plasmonic nanostructures are left positively charged after "hot electron" injection in the neighboring semiconductor. An electron donor solution or HTM needs to be in contact with them in order to replenish their carrier concentration, and to obtain a sustained and stable photoexcited current. The choice of an adequate electron donor material is critical to guarantee this process. In their pioneering works, Tatsuma *et al.*[18] brought plasmonic Au nanoparticles in contact with different donor solutions including $[Fe(CN)6]^{4-}$, I^-, Fe^{2+}, ferrocenecarboxylic acid, Br^-, 1,1'-ferrocenedicarboxylic acid and Cl^-. They reported a IPCE of 12 % at around 560 nm when using Fe^{2+} as electron donor and an stunning 26 % upon addition of 4-nitrobenzoic acid, probably because it gets absorved in the exposed TiO_2 and blocks the recombination of electrons. Nevertheless, other factors such as the regeneration rate that these solutions provide needs to be considered. Tian *et al.*[52, 54], showed that the performance of donor solutions containing $[Fe(CN)6]^{4-}$, Fe^{2+} and ferrocenecarboxylic acid does not only depend on their apparent formal potential. Transient absorbance measurements clearly indicate different regeneration rates in these solutions, Fe^{2+} being the fastest one. This result is in agreement with Tatsuma's findings[18].

Carrier regeneration using liquid electrolytes is adequate for photocatalysis applications as it facilitates the flow of chemicals to be processed in contact with the plasmonic nanostructures. Nevertheless, liquid cells are unpractical for photovoltaic applications due to lack of stability, leaking and evaporation issues. In recent years, several solid state plasmonic solar cell structures have been proposed, bringing a practical application one step

closer. Initial attempts to fabricate solid state photovoltaic cells by using organic and inorganic HTMs were unsatisfactory, due to the very low efficiencies obtained, around four orders of magnitude lower than liquid cells using an electrolyte containing a redox couple[51]. Tatsuma *et al.*[51] tested different solid state cell architectures composed by Au nanoparticles in contact with TiO_2 using different HTM materials such as PVK, TPD, CuI and CuSCN (see abbreviations section). A very low maximum IPCE value of 0.0024% was obtained using PVK. This considerably lower efficiency was explained as a consequence of contact between the HTM and TiO_2, giving rise to recombination between electrons in the TiO_2 layers and holes in the HTM material. Possible degradation of the HTM layers was also considered.

Surprisingly, subsequent studies not including any specific electrolyte or HTM layer resulted in higher efficiencies. Tatsuma *et al.*[97, 98] showed that devices composed by Au and Ag nanoparticles on TiO_2 and in contact with ITO, where electrons are simply injected into the nanoparticles from the ITO film, can achieve IPCE values around 0.4% and 0.6 % for Au and Ag nanoparticles respectively [Figure 10]. Solid state solar cells with considerably higher efficiencies were recently obtained by Tian *et al.*[52] by using a similar architecture consisting of Au nanoparticles on TiO_2 and polyethylene oxide (PEO) filled with TiO_2 nanoparticles as HTM, which contains optimized redox couples I^-/I^-_3. They reported IPCE values as high as 6 %. Recently, Reineck *et al.*[99] used Spiro-OMeTAD as HTM film on solid state cells with self assembled Au and Ag nanoparticles, obtaining IPCE values of 4.9 and 3.8 % respectively. While recent advances in this field are encouraging, further research is needed in order to obtain HTMs and architectures that avoid carrier recombination due to direct contact with the semiconducting material.

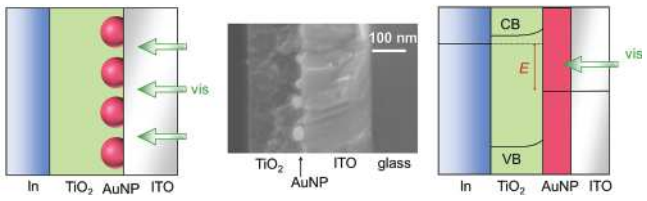

Figure 10. Solid state plasmonic photovoltaic cell consisting of In/TiO_2/Au nanoparticles/ITO. Figures reproduced with permission from ref. [97]. © 2011 American Institute of Physics.

4.6. Other applications and approaches

The plasmonic charge separation and injection of "hot electrons" processes from plasmonic nanoparticles into the semiconductor matrix significantly changes the conductivity of the system upon illumination. Some works have explored the possibility of using this principle to obtain plasmoelectronic devices, with conductivity controlled by the intensity of the visible light illumination. Grzybowski *et al.*[100, 101] observed this effect in nanoparticles stabilized with different self assembled monolayers that increase or decrease the electrical conductivity of the material during resonance depending on whether these contain neutral or charged ligands respectively. In a similar note, Mubeen *et al.*[102] investigated devices consisting of multilayers of Au nanoparticles and TiO_2. The tunneling of photoexcited "hot electrons" in the Au nanoparticles produced an over 1000-fold increase in conductance when illuminated at 600 nm over that of TiO_2 films with no Au nanoparticles. Son *et*

al.[103] reported surface plasmon enhanced photoconductance in TiO_2 nanofibers loaded with Au nanoparticles. Several other works have focused on observing plasmonic photoinduced currents in nanodiode structures. Lee *et al.* [37] observed an enhancement in the photocurrent due to plasmon assisted generation of "hot electrons" on nanodiodes consisting of gold islands on TiO_2, that can also be further enhanced with dye molecules[104]. Knight *et al.* [105] observed "hot electron" flows generated by photons in the infrared range in Au/Si nanoantenas. The reciprocal effect, *i.e.* manipulation of plasmonic resonance by changing the electronic density has been proposed for applications such as smart windows and displays[106].

Interestingly, very few works have been presented to date on plasmonic charge separation using prorogating SPPs. In their pioneering work, Wang et *al.*[107] proposed a new architecture based on SPP excitation in a metal-insulator-metal (MIM) structure illuminated under the prism coupler configuration, also known as Kretschmann configuration [Figure 11(a)]. Owing to the high localization of SPP on the top metal thin film, more "hot electrons" are transmitted from the top electrode to the bottom than in the contrary direction, leading to the detection of a net photocurrent. Figure 11 (b) shows that maximum photocurrent is obtained at the incident angle that allows matching of the incoming light with propagating SPPs, demonstrating that these are key in the carrier separation process. Their calculations suggest that this kind of architecture could achieve efficiencies up to 4.3 % with 640 nm radiation using Ag, due to its longer mean free path as compared with Au, which only would achieve a 3.5 % at 780 nm. Nevertheless, they were only able to measure efficiency values around 2.7 % due to surface recombination at the metal-insulator interface. Along the same lines, Pradhan *et al.*[108] investigated semiconductor-insulator-semiconductor hetero-junctions consisting of Al:ZnO/SiO_2/Si. The use of propagating SPPs is interesting since they cannot decay directly into photons unless roughness is present at the surface[109], making non-radiative decay the only mechanism possible in very flat plasmonic films.

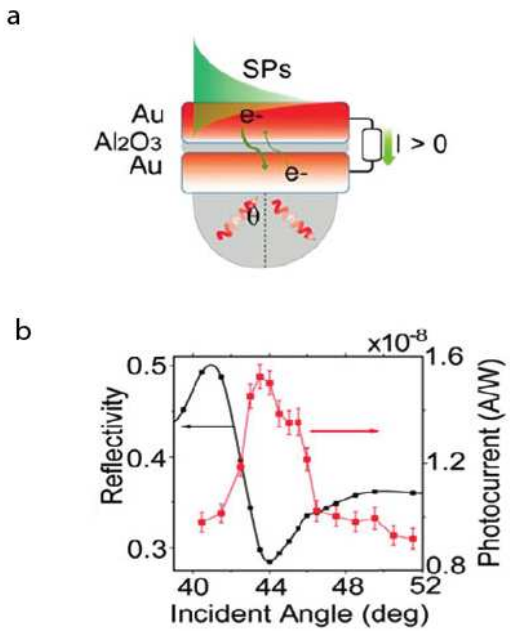

Figure 11. Plasmonic charge separation using prorogating surface plasmon polaritons (SPP): (a) Sketch of metal-insulator-metal device able to generate photocurrents thanks to the excitation of propagating SPPs. (b) Maximum photocurrent is obtained when SPP are excited on the top metal film. Figures reproduced with permission from ref. [107]. © 2011 American Chemical Society.

5. New directions in Plasmonic energy conversion

As shown in previous sections, plasmonic energy conversion has been demonstrated and the photon-to-electron conversion efficiencies obtained have been largely improved in the last few years. Initial experiments carried out using electron donor solutions were followed by solid state devices using HTMs. However, this technology has still a long way to go in order to approach the record efficiencies achieved by state-of-the-art semiconductor solar cells. Several aspects directly related to the nature of these devices need to be considered, including the materials used in the fabrication of the plasmonic nanostructures, the semiconductor materials used to capture the photoexcited "hot electrons", their architecture and even the fabrication methods used. In this section, some of the most important aspects that need major advancements to push further the efficiency of this energy conversion method are reviewed and discussed.

5.1. Plasmonic energy conversion efficiency

A very important point that needs to be carefully considered is the efficiency of the plasmonic energy conversion process. As shown in section 3.2, the energy from the surface plasmons $\hbar\omega_p$ can decay and be transferred to electrons in the whole DOS of the nanostructure conduction band. This creates a very broad distribution of "hot electron" states above the Fermi energy, many of which have insufficient energy to be injected into the semiconductor. White *et al.*[110] estimated the efficiency limit of Schottky barrier based plasmonic energy conversion devices. They considered a parabolic DOS for the conduction band of metals such as Ag and Au, as shown in Figure 3 (b), and an adjacent semiconductor forming a Schottky barrier of ϕ_{SB}=1.2 eV. A maximum IPCE of 8 % is obtained when considering equal probability of photoexcitation for all the electrons in the conduction band. Nevertheless, photoemission experiments in noble metals indicate that electrons close to the Fermi energy are excited preferentially over lower energy electrons[111], which considerably increases the efficiency of this process. Further engineering of the DOS of the plasmonic material to favor preferential excitation of electronic levels close to the Fermi energy will allow efficiencies in excess of 22 % [110]. This would be the case, for example, of semiconductor based plasmonic nanostructures, where the band-gap determines the final energy of the photoexcited electrons. Other factors such as the height of the Schottky barrier considerably affect the efficiency of the process, and thus the semiconductor material needs to be also carefully selected. In the following sections, several considerations regarding the materials used in plasmonic energy conversion devices aimed at increasing the energy conversion efficiency will be detailed.

5.2. Plasmonic materials: from metals to conducting oxides

So far, noble metals such as Ag and Au have been virtually the only materials used in plasmonic energy conversion. Noble metal nanostructures exhibit very intense surface plasmon excitations that give rise to very strong light absorption, mainly in the visible range. The frequency at which plasmonic nanostructures undergo surface plasmon resonance strongly depends on their carrier concentration. For spherical nanoparticles[30], surface plasmon resonance takes place at a frequency $\omega_{LSPR} \sim \omega_p/\sqrt{3}$, where the plasma frequency ω_p directly depends on the concentration of carriers n_e as follows:

$$\omega_p = \sqrt{\frac{n_e e^2}{m^* \varepsilon_0}}$$

where *e* is the charge of the electron, *m** is the effective mass of the electron and ε_0 is the permittivity of free-space. Figure 12 shows the calculated optical absorption for different metal nanoparticles such as Al, Ag, Au and Cu versus the solar spectral irradiance AM1.5. Indeed, very narrow absorptions are observed in the lower part of the visible range due to their relatively high carrier concentrations[112] (around 5.9 x 10^{22} cm^{-3} for Ag and Au). Nevertheless, a significant part of radiation from the Sun that reaches the surface of Earth has longer wavelengths, in the near infrared range. Indeed, the solar radiation with wavelengths longer than 800 nm accounts for around 40 % of the total solar energy received from Sun[46]. The limited portion of the solar spectrum being used drastically limits the applicability of this energy conversion method. It is therefore of paramount importance to find materials that will allow using a more significant portion of the solar spectrum. In this scope, it is worth noticing that materials with lower carrier concentrations have also lower plasma frequencies, and thus their resonance takes place at longer wavelengths. Conducting oxides are thus well suited to extend the absorption range toward the near infrared range owing to their lower carrier concentrations. Figure 12 shows the calculated optical extinction (*i.e.* optical absorption) for several broadly used conducting oxides such as RuO_2, aluminum doped zinc oxide (AZO) and tin-doped indium oxide (ITO). The absorption of light by conducting oxides is spectrally broader than in noble metals, mainly due to their higher optical losses[113]. This fact is remarkable since it considerably increases the range of wavelengths that can excite surface plasmon resonance in a given nanostructure. “Hot electron” generation by conducting oxide plasmonic nanostructures remains largely unexplored. The use of plasmonic nanostructures made out of conducting oxides to capture and convert the infrared zone of the spectrum could extend the range of applications of plasmonic solar cells, significantly increasing their overall efficiency.

Different conducting oxides can be used in order to achieve conversion in selected areas of the spectrum as shown in Figure 12. In addition, for the case of heavily doped conducting oxides such as AZO and ITO, it is possible to use their doping concentration in order to tune the carrier concentration, and thus the region of the spectrum where plasmonic resonance takes place. For example, the concentration of carriers in AZO can be varied from 0.5 to 10 x 10^{20} cm^{-3} changing the concentration of Al, giving rise to a strong variation in the position of the surface plasmon resonance from 2200 nm to 880 nm[114], as shown in Figure 12. In addition, inspired by multiple junction solar cells, in which semiconductors with different band-gaps are combined in order to cover the whole solar spectrum, systems combining multiple metals and conducting oxides can be explored in order to adapt the absorption spectrum of the devices to that of the solar radiation.

Other approaches can be taken in order to further engineer the band structure and density of carriers of the plasmonic nanostructures, such as using heavily doped semiconductors other than the conducting oxides previously mentioned[115, 116]. Also, it is possible to create alloys of two or more metals with fine tuned plasmonic properties[115]. In this sense, noble-transition metal alloys are the best candidates for this application since they allow modifying the Fermi level and the surface plasma frequency ω_p of the nanostructures. Other materials such as conducting transition metal nitrides including TiN, ZrN, HfN and TaN[117, 118], are interesting for plasmonic applications since they exhibit metallic properties in the visible frequencies[117, 118].

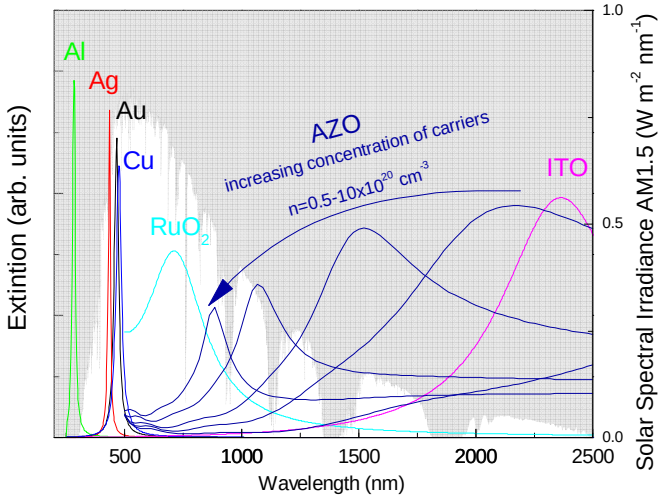

Figure 12. Optical extinction of plasmonic nanostructures made out of metals (Al, Ag, Au and Cu) and conducting oxides (RuO_2, AZO and ITO). While metals absorb in a narrow visible range, conducting oxides have a much broader extinction spectra, extending from the visible range to the near infrared. Different doping levels of AZO allow tuning of the carrier concentration and thus the absorption zone. The solar irradiance spectrum is plotted in white in the background.

5.3. Semiconductor materials for "hot electron" injection: wide band-gap semiconductors

The choice of an adequate semiconductor to trap the photoexcited "hot electrons" greatly impacts the charge injection mechanisms. Important factors are the band gap of the semiconductor, which affects the height of the semiconductor-metal Schottky barrier, and the density of available states in the conduction band, which affects the efficiency of the "hot electron" injection process. Good alignment of the plasmonic nanostructures Fermi level with the bands of the semiconductor is important to favor efficient carrier injection[33]. The Fermi energy level is around 0 V on the normal hydrogen electrode (NHE) scale[14] for noble metals and conducting oxides, as shown in Figure 13. The energy that surface plasmons transfer to "hot electrons" upon decay ranges between 1.0 and 4.0 eV with respect to the Fermi level depending on the material and surface plasmon resonance frequency. Thus, the conduction band of the electron acceptor semiconductor needs to be close enough so that the photoexcited "hot electrons" can overcome the Schottky barrier ϕ_{SB}. Figure 13 depicts the position of the conduction and valence bands of several wide band-gap semiconductors of interest for plasmonic energy conversion with respect to the Fermi energy of a selection of metals and conducting oxides. A considerable part of the photoexcited "hot electrons" can be lost in the Schottky barrier if this is too high, leading to considerable loss in energy efficiency. Regarding the density of available states in the conduction band, TiO_2 is a wide band gap semiconductor (E_g = 3.3 eV) that has been widely used in dye sensitized solar cells. It has a well known good electron-accepting capability due to its high density of states in the conduction band. These characteristics make it an excellent candidate for this application. Nevertheless, other semiconductors such as ZnO, CeO_2 and AgBr have their conduction and valence bands adequately positioned and can also serve as efficient electron acceptors. Comparative studies will be needed to determine the most adequate material considering the particular characteristics of the plasmonic nanostructures used.

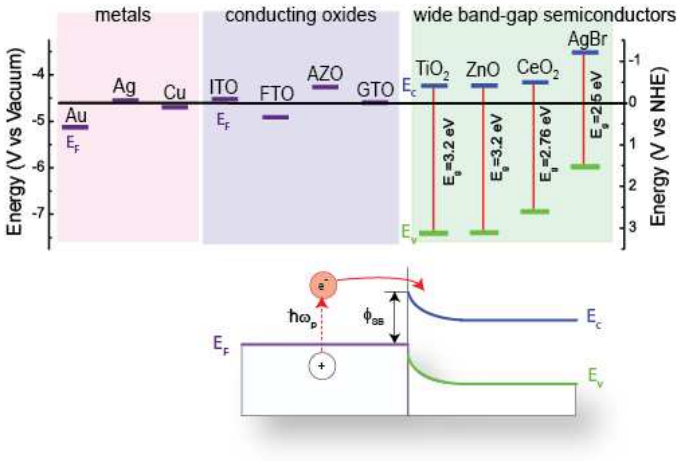

Figure 13. Semiconductor materials for "hot electron" collection. Fermi level (E_F), conduction (E_c) and valence (E_v) bands energy for selected metals, conducting oxides and wide band-gap semiconductors of interest for the fabrication of plasmonic nanostructures. The energy values are plotted on a potential scale (V) versus the normal hydrogen electrode (NHE) and also potential (V) versus vacuum.

5.4. Fabrication methods

So far, the fabrication of plasmonic energy conversion devices has been vastly dominated by solution based methods, where commercially available noble metal and semiconductor nanoparticles are properly combined[17, 18, 50-52, 56]. Noble metal nanoparticles of controlled size are also obtained using photocatalysis[54, 65, 68, 72, 74, 96, 119], electrodeposition[69, 97], electrodeposition through a thin alumina nanomask[98], electrostatic self-assembly[99] and modified Turkevich method[68, 120]. More complicated structures such as, for example, core-shell nanoparticles have been fabricated via a hydrothermal treatment of TiF_4 precursor using noble metal colloid particles[93, 94]. Also, noble metal nanoparticle decorated TiO_2 nanotubes have been fabricated through hydrothermal method[80] and electrochemical anodic oxidation[78, 83]. Surprisingly, only a few studies have applied lithography methods to achieve more elaborated plasmonic nanostructures shapes such as nanorods[46, 62], nanoprisms[95] and nanowires[67]. While the above mentioned techniques are relevant to provide proof of concept of this energy conversion method, scalable techniques providing a high degree of homogeneity over larger areas and fine control of the nanostructures size will be needed in order to allow further development and eventually commercialization of these kinds of devices. In this scope, physical vapor deposition (PVD) based techniques modified for the creation of nanoparticles from a high pressure plasma are excellent candidates for this application[121-123]. For example, terminated cluster growth is a PVD based method consisting of magnetron sputtering at elevated pressures, giving rise to condensation and formation of nanoparticles of controlled size and composition[124]. Furthermore, insertion of reactive gases such as oxygen can lead to deformation of oxide nanoparticles such as TiO_2[125, 126]. After generation, the nanoparticles are slightly charged which allows for further control of their size by for example using a RF quadrupole[121]. The use of these kinds of techniques could lead to important breakthroughs in the development of this technology.

6. Outlook and conclusions

As it has been shown in this review, plasmonic conversion of solar energy offers great promise as a new method of energy transformation, mainly due to the outstanding light trapping and "hot electron" generation properties of surface plasmons. Several factors directly related to the fundamental nature, the materials involved and the architectures used in this novel energy conversion method affect strongly its efficiency and have been discussed in detail within this review. Efficient absorption of light over the whole solar spectrum is an important factor that will determine the applicability of this method in photovoltaic devices. The plasmonic nanostructures investigated so far, mainly made out of noble metals, are able to convert light only from a quite narrow region of the visible spectrum. Research aimed at using other materials able to capture and convert light in the infrared range, such as conducting oxides and semiconductors, will allow further development of these kinds of devices. Additionally, combination of nanostructures made out of different strategically selected materials will eventually allow using the whole solar spectrum. Further engineering of the DOS of the plasmonic material to favor preferential excitation of electronic levels close to the Fermi energy will allow pushing further the efficiency limits.

Significant research also needs to be carried out to optimize the architecture of these devices. Factors such as size and shape of the plasmonic nanostructures play a predominant role to guarantee efficient surface plasmon excitation, strong concentration of electromagnetic fields and, for hence, efficient creation of "hot electrons". So far, only a few studies have focused on the role of size and shape of the plasmonic structures in the efficiency of the energy conversion. Following to surface plasmon decay, fast extraction of the photoexcited "hot electrons" and injection in the neighboring semiconductor before electron-electron scattering takes place in the femtosecond timescale is very important to boost the energy conversion efficiency. Utilization of semiconducting materials forming an adequate Schottky barrier with the plasmonic nanostructures and with abundant available states in their conduction bands is instrumental to achieve this goal. Comparative studies investigating different semiconductors materials depending on the characteristics of the plasmonic nanostructures used and the radiation converted need to be carried out.

The last step in this energy conversion method, *i.e.* carrier regeneration using a donor solution or a HTM, is also very relevant. Fast regeneration of carriers allows maintaining the energy conversion mechanism. While donor solutions have been demonstrated to achieve high IPCE efficiencies up to 26 %, considerable research needs to be performed in this field to obtain reliable solid HTMs compatible with conventional photovoltaic devices. In addition, recombination of carriers by contact between the HTM and the semiconductor needs to be avoided by, for example, minimizing the contact surface between them, or by passivating the semiconductor exposed surface. Finally, but not less important, different fabrication methods that will allow controlled, homogeneous fabrication of plasmonic nanostructures and the rest of the layers involved in these kinds of devices need to be overtaken. While solution based methods have shown great flexibility, PVD-based fabrication methods offer promising opportunities in this field mainly due to their ability to obtain plasmonic nanostructures with high control of their size and composition.

While still in its infancy, considerable progress has been made so far in the field of plasmonic solar energy conversion, opening a new venue for photovoltaic and photocatalytic devices. However, significant advances in the previously detailed fields will allow pushing further the efficiency of this method.

7. Acknowledgements

C.C. acknowledges Andre Anders and Rueben Mendelsberg for insightful discussions. This work was supported by the Assistant Secretary for Energy Efficiency and Renewable Energy, Office of Building Technology, of the US Department of Energy under Contract No. DE-AC02-05CH11231.

8. Disclaimer

9. Abbreviations

AM1.5: air mass coefficient for 1.5 atmosphere thickness, corresponding to a solar zenith angle of z=48.2°
AZO: aluminum doped zinc oxide
DOS: density of states
HTM: hole transporting material
IPCE: incident photon-to-electron conversion efficiency
ITO: tin-doped indium oxide
LSPR: localized surface plasmon resonance
MIM: metal-insulator-metal
N3: cis-bis(4,4'-dicarboxy-2,2'-bipyridine)dithiocyanato ruthenium(II)
NHE: normal hydrogen electrode
NPD: 4,4-bis[N-(1-naphthyl)-N-phenyl-amino]biphenyl
PEO: polyethylene oxide

PVD: physical vapor deposition
PVK: poly(N-vinilcarbazole)
Spiro-OMeTAD: (2,2(,7,7(-tetrakis-(N,N-di-pmethoxyphenylamine)9,9(-spirobifluorene)
SPP: surface plasmon polariton
TiO_2: titanium dioxide
TPD: N,N'-diphenyl-N,N'-bis(3-methylphenyl)-(1,1'-biphenyl)-4,4'-diamine

10. References

1. H. Raether, *Surface Plasmons on smooth and rough surfaces and on gratings*. (Springer-Verlag, Berlin, 1986).
2. W. L. Barnes, A. Dereux and T. W. Ebbesen, Nature **424** (6950), 824-830 (2003).
3. H. A. Atwater, Scientific American **April**, 56-63 (2007).
4. D. K. Gramotnev and S. I. Bozhevolnyi, Nat Photon **4** (2), 83-91 (2010).
5. Y. Wang, E. W. Plummer and K. Kempa, Advances in Physics **60** (5), 799-898 (2011).
6. N. Engheta, Science **317** (5845), 1698-1702 (2007).
7. A. L. Falk, F. H. L. Koppens, C. L. Yu, K. Kang, N. de Leon Snapp, A. V. Akimov, M.-H. Jo, M. D. Lukin and H. Park, Nat Phys **5** (7), 475-479 (2009).
8. J. A. Schuller, E. S. Barnard, W. Cai, Y. C. Jun, J. S. White and M. L. Brongersma, Nat Mater **9** (3), 193-204 (2010).
9. J. Homola, S. S. Yee and G. Gauglitz, Sensors and Actuators B: Chemical **54** (1-2), 3-15 (1999).
10. Basic Research Needs for Solar Energy Utilization, Basic Energy Science Advisory Committe (BESAC), (2005), http://science.energy.gov/~/media/bes/pdf/reports/files/seu_rpt_print.pdf.
11. S. Pillai and M. A. Green, Solar Energy Materials and Solar Cells **94** (9), 1481-1486 (2010).
12. M. J. Mendes, A. Luque, I. Tobias and A. Marti, Applied Physics Letters **95** (7), 071105-071103 (2009).
13. H. A. Atwater and A. Polman, Nat Mater **9** (3), 205-213 (2010).
14. S. Linic, P. Christopher and D. B. Ingram, Nat Mater **10** (12), 911-921 (2011).
15. S. Mokkapati and K. R. Catchpole, Journal of Applied Physics **112** (10), 101101-101119 (2012).
16. G. Zhao, H. Kozuka and T. Yoko, Thin Solid Films **277** (1–2), 147-154 (1996).
17. Y. Tian and T. Tatsuma, Chemical Communications (16), 1810-1811 (2004).
18. Y. Tian and T. Tatsuma, Journal of the American Chemical Society **127** (20), 7632-7637 (2005).
19. Z. Xuming, C. Yu Lim, L. Ru-Shi and T. Din Ping, Reports on Progress in Physics **76** (4), 046401 (2013).
20. W. Hou and S. B. Cronin, Advanced Functional Materials, n/a-n/a (2012).
21. S. C. Warren and E. Thimsen, Energy & Environmental Science **5** (1), 5133-5146 (2012).
22. E. W. McFarland and J. Tang, Nature **421** (6923), 616-618 (2003).
23. M. A. Green, K. Emery, Y. Hishikawa, W. Warta and E. D. Dunlop, Progress in Photovoltaics: Research and Applications **20** (1), 12-20 (2012).
24. H. Yuen, M. Wiemer and V. Sabnis, in *Renewable Energy and the Environment* (Optical Society of America, 2011), pp. SRWB3.
25. A. Polman and H. A. Atwater, Nat Mater **11** (3), 174-177 (2012).
26. J. W. Gadzuk, The Journal of Physical Chemistry B **106** (33), 8265-8270 (2002).
27. H. Nienhaus, Surface Science Reports **45** (1–2), 1-78 (2002).
28. B. O'Regan and M. Gratzel, Nature **353** (6346), 737-740 (1991).
29. M. Gratzel, Nature **414** (6861), 338-344 (2001).

30. U. Kreibig and M. Vollmer, *Optical properties of metal clusters*. (Berlin, Heidelberg, 1995).
31. E. Verhagen, A. Polman and L. Kuipers, Opt. Express **16** (1), 45-57 (2008).
32. P. K. Jain, K. S. Lee, I. H. El-Sayed and M. A. El-Sayed, The Journal of Physical Chemistry B **110** (14), 7238-7248 (2006).
33. S. K. Cushing, J. Li, F. Meng, T. R. Senty, S. Suri, M. Zhi, M. Li, A. D. Bristow and N. Wu, Journal of the American Chemical Society **134** (36), 15033-15041 (2012).
34. C. Wadell, T. J. Antosiewicz and C. Langhammer, Nano Letters (2012).
35. P. Christopher, H. Xin and S. Linic, Nat Chem **3** (6), 467-472 (2011).
36. H. Hertz, Annalen der Physik **267** (8), 983-1000 (1887).
37. Y. K. Lee, C. H. Jung, J. Park, H. Seo, G. A. Somorjai and J. Y. Park, Nano Letters **11** (10), 4251-4255 (2011).
38. C. Sönnichsen, T. Franzl, T. Wilk, G. von Plessen, J. Feldmann, O. Wilson and P. Mulvaney, Physical Review Letters **88** (7), 077402 (2002).
39. J. Hofmann and W. Steinmann, Physica Status Solidi (b) **30** (1), K53-K56 (1968).
40. J. G. Endriz and W. E. Spicer, Physical Review Letters **24** (2), 64-68 (1970).
41. T. A. Callcott and E. T. Arakawa, Physical Review B **11** (8), 2750-2758 (1975).
42. J. T. Stuckless and M. Moskovits, Physical Review B **40** (14), 9997-9998 (1989).
43. J. Lehmann, M. Merschdorf, W. Pfeiffer, A. Thon, S. Voll and G. Gerber, Physical Review Letters **85** (14), 2921-2924 (2000).
44. Z. Zhang and J. T. Yates, Chemical Reviews **112**, 5520-5551 (2012).
45. M. Moskovits, Science **332** (6030), 676-677 (2011).
46. Y. Nishijima, K. Ueno, Y. Yokota, K. Murakoshi and H. Misawa, The Journal of Physical Chemistry Letters **1** (13), 2031-2036 (2010).
47. Y. Ohko, T. Tatsuma, T. Fujii, K. Naoi, C. Niwa, Y. Kubota and A. Fujishima, Nat Mater **2** (1), 29-31 (2003).
48. K. Naoi, Y. Ohko and T. Tatsuma, Journal of the American Chemical Society **126** (11), 3664-3668 (2004).
49. T. Hirakawa and P. V. Kamat, Langmuir **20** (14), 5645-5647 (2004).
50. K. Yu, Y. Tian and T. Tatsuma, Physical Chemistry Chemical Physics **8** (46), 5417-5420 (2006).
51. K. Yu, N. Sakai and T. Tatsuma, Electrochemistry Communications (76), 161 (2008).
52. Y. Tian, X. Shi, C. Lu, X. Wang and S. Wang, Electrochemistry Communications **11** (8), 1603-1605 (2009).
53. A. Furube, L. Du, K. Hara, R. Katoh and M. Tachiya, Journal of the American Chemical Society **129** (48), 14852-14853 (2007).
54. Y. Tian, X. Wang, D. Zhang, X. Shi and S. Wang, Journal of Photochemistry and Photobiology A: Chemistry **199** (2–3), 224-229 (2008).
55. L. Du, A. Furube, K. Hara, R. Katoh and M. Tachiya, Journal of Photochemistry and Photobiology C: Photochemistry Reviews (0) (2012).
56. L. Du, A. Furube, K. Yamamoto, K. Hara, R. Katoh and M. Tachiya, The Journal of Physical Chemistry C **113** (16), 6454-6462 (2009).
57. J. Hohlfeld, S. S. Wellershoff, J. Güdde, U. Conrad, V. Jähnke and E. Matthias, Chemical Physics **251** (1–3), 237-258 (2000).
58. H. Inouye, K. Tanaka, I. Tanahashi and K. Hirao, Physical Review B **57** (18), 11334-11340 (1998).
59. K. Puech, F. Z. Henari, W. J. Blau, D. Duff and G. Schmid, Chemical Physics Letters **247** (1–2), 13-17 (1995).
60. C. Langhammer, Z. Yuan, I. Zorić and B. Kasemo, Nano Letters **6** (4), 833-838 (2006).
61. K. Ueno and H. Misawa, Journal of Photochemistry and Photobiology A: Chemistry **221** (2–3), 130-137 (2011).
62. Y. Nishijima, K. Ueno, Y. Kotake, K. Murakoshi, H. Inoue and H. Misawa, The Journal of Physical Chemistry Letters **3** (10), 1248-1252 (2012).
63. S. Mubeen, J. Lee, N. Singh, S. Kramer, G. D. Stucky and M. Moskovits, Nat Nano **advance online publication** (2013).

64. D. B. Ingram, P. Christopher, J. L. Bauer and S. Linic, ACS Catalysis **1** (10), 1441-1447 (2011).
65. E. Kazuma, N. Sakai and T. Tatsuma, Chemical Communications **47** (20), 5777-5779 (2011).
66. E. Kazuma and T. Tatsuma, The Journal of Physical Chemistry C (2012).
67. M. W. Knight, Y. Wang, A. S. Urban, A. Sobhani, B. Y. Zheng, P. Nordlander and N. J. Halas, Nano Letters (2013).
68. T. Lana-Villarreal and R. Gómez, Chemical Physics Letters **414** (4–6), 489-494 (2005).
69. N. Sakai, Y. Fujiwara, Y. Takahashi and T. Tatsuma, ChemPhysChem **10** (5), 766-769 (2009).
70. G. Valverde-Aguilar, J. García-Macedo, V. Rentería-Tapia and M. Aguilar-Franco, Applied Physics A: Materials Science & Processing **103** (3), 659-663 (2011).
71. C. Gomes Silva, R. Juárez, T. Marino, R. Molinari and H. García, Journal of the American Chemical Society **133** (3), 595-602 (2010).
72. E. Kowalska, O. O. P. Mahaney, R. Abe and B. Ohtani, Physical Chemistry Chemical Physics **12** (10), 2344-2355 (2010).
73. Y. Ide, M. Matsuoka and M. Ogawa, Journal of the American Chemical Society **132** (47), 16762-16764 (2010).
74. T. Toyoda, S. Tsugawa and Q. Shen, Journal of Applied Physics **105** (3), 034314 (2009).
75. E. Kowalska, R. Abe and B. Ohtani, Chemical Communications (2), 241-243 (2009).
76. A. Tanaka, A. Ogino, M. Iwaki, K. Hashimoto, A. Ohnuma, F. Amano, B. Ohtani and H. Kominami, Langmuir **28** (36), 13105-13111 (2012).
77. X. Shi, K. Ueno, N. Takabayashi and H. Misawa, The Journal of Physical Chemistry C (2012).
78. F. Wu, X. Hu, J. Fan, E. Liu, T. Sun, L. Kang, W. Hou, C. Zhu and H. Liu, Plasmonics, 1-8 (2012).
79. International Journal of Photoenergy **2012** (2012).
80. D. Gong, W. C. J. Ho, Y. Tang, Q. Tay, Y. Lai, J. G. Highfield and Z. Chen, Journal of Solid State Chemistry **189** (0), 117-122 (2012).
81. N. Sakai, T. Sasaki, K. Matsubara and T. Tatsuma, Journal of Materials Chemistry **20** (21), 4371-4378 (2010).
82. Y. Shiraishi, D. Tsukamoto, Y. Sugano, A. Shiro, S. Ichikawa, S. Tanaka and T. Hirai, ACS Catalysis **2** (9), 1984-1992 (2012).
83. K. Chen, X. Feng, R. Hu, Y. Li, K. Xie, Y. Li and H. Gu, Journal of Alloys and Compounds **554** (0), 72-79 (2013).
84. Z. H. Chen, Y. B. Tang, C. P. Liu, Y. H. Leung, G. D. Yuan, L. M. Chen, Y. Q. Wang, I. Bello, J. A. Zapien, W. J. Zhang, C. S. Lee and S. T. Lee, The Journal of Physical Chemistry C **113** (30), 13433-13437 (2009).
85. H. M. Chen, C. K. Chen, C.-J. Chen, L.-C. Cheng, P. C. Wu, B. H. Cheng, Y. Z. Ho, M. L. Tseng, Y.-Y. Hsu, T.-S. Chan, J.-F. Lee, R.-S. Liu and D. P. Tsai, Acs Nano **6** (8), 7362-7372 (2012).
86. Z. Han, L. Wei, Z. Zhang, X. Zhang, H. Pan and J. Chen, Plasmonics, 1-10 (2013).
87. A. Primo, T. Marino, A. Corma, R. Molinari and H. García, Journal of the American Chemical Society **133** (18), 6930-6933 (2011).
88. H. Kominami, A. Tanaka and K. Hashimoto, Chemical Communications **46** (8), 1287-1289 (2010).
89. X. Zhou, C. Hu, X. Hu, T. Peng and J. Qu, The Journal of Physical Chemistry C **114** (6), 2746-2750 (2010).
90. C. Hu, T. Peng, X. Hu, Y. Nie, X. Zhou, J. Qu and H. He, Journal of the American Chemical Society **132** (2), 857-862 (2009).
91. P. Wang, B. Huang, X. Qin, X. Zhang, Y. Dai, J. Wei and M.-H. Whangbo, Angewandte Chemie **120** (41), 8049-8051 (2008).
92. S. T. Kochuveedu, D.-P. Kim and D. H. Kim, The Journal of Physical Chemistry C **116** (3), 2500-2506 (2011).
93. N. Zhang, S. Liu, X. Fu and Y.-J. Xu, The Journal of Physical Chemistry C **115** (18), 9136-9145 (2011).
94. Z. Zheng, B. Huang, X. Qin, X. Zhang, Y. Dai and M.-H. Whangbo, Journal of Materials Chemistry **21** (25), 9079-9087 (2011).

95. C. Xiaoqing, L. Peng, T. Hua, K. Tetsuya and Y. Jinhua, Science and Technology of Advanced Materials **12** (4), 044604 (2011).
96. Z. Zhang, L. Zhang, M. N. Hedhili, H. Zhang and P. Wang, Nano Letters **13** (1), 14-20 (2012).
97. Y. Takahashi and T. Tatsuma, Applied Physics Letters **99** (18), 182110-182113 (2011).
98. Y. Takahashi and T. Tatsuma, Nanoscale **2** (8), 1494-1499 (2010).
99. P. Reineck, G. P. Lee, D. Brick, M. Karg, P. Mulvaney and U. Bach, Advanced Materials **24** (35), 4750–4755 (2012).
100. H. Nakanishi, K. J. M. Bishop, B. Kowalczyk, A. Nitzan, E. A. Weiss, K. V. Tretiakov, M. M. Apodaca, R. Klajn, J. F. Stoddart and B. A. Grzybowski, Nature **460** (7253), 371-375 (2009).
101. S. C. Warren, D. A. Walker and B. A. Grzybowski, Langmuir **28** (24), 9093-9102 (2012).
102. S. Mubeen, G. Hernandez-Sosa, D. Moses, J. Lee and M. Moskovits, Nano Letters **11** (12), 5548-5552 (2011).
103. M.-S. Son, J.-E. Im, K.-K. Wang, S.-L. Oh, Y.-R. Kim and K.-H. Yoo, Applied Physics Letters **96** (2), 023115 (2010).
104. Y. K. Lee, J. Park and J. Y. Park, The Journal of Physical Chemistry C (2012).
105. M. W. Knight, H. Sobhani, P. Nordlander and N. J. Halas, Science **332** (6030), 702-704 (2011).
106. G. Garcia, R. Buonsanti, E. L. Runnerstrom, R. J. Mendelsberg, A. Llordes, A. Anders, T. J. Richardson and D. J. Milliron, Nano Letters **11** (10), 4415-4420 (2011).
107. F. Wang and N. A. Melosh, Nano Letters **11** (12), 5426-5430 (2011).
108. A. K. Pradhan, T. Holloway, R. Mundle, H. Dondapati and M. Bahoura, Applied Physics Letters **100** (6), 061127 (2012).
109. T. Inagaki, K. Kagami and E. T. Arakawa, Physical Review B **24** (6), 3644-3646 (1981).
110. T. P. White and K. R. Catchpole, Applied Physics Letters **101** (7), 073905 (2012).
111. C. N. Berglund and W. E. Spicer, Physical Review **136** (4A), A1044-A1064 (1964).
112. C. Kittel, *Introduction to solid state physics / Charles Kittel*. (Wiley, New York :, 1976).
113. H. Hövel, S. Fritz, A. Hilger, U. Kreibig and M. Vollmer, Physical Review B **48** (24), 18178-18188 (1993).
114. R. J. Mendelsberg, S. H. N. Lim, Y. K. Zhu, J. Wallig, D. J. Milliron and A. Anders, Journal of Physics D: Applied Physics **44** (23), 232003 (2011).
115. P. R. West, S. Ishii, G. V. Naik, N. K. Emani, V. M. Shalaev and A. Boltasseva, Laser & Photonics Reviews **4** (6), 795-808 (2010).
116. A. J. Hoffman, L. Alekseyev, S. S. Howard, K. J. Franz, D. Wasserman, V. A. Podolskiy, E. E. Narimanov, D. L. Sivco and C. Gmachl, Nat Mater **6** (12), 946-950 (2007).
117. G. V. Naik, J. L. Schroeder, X. Ni, A. V. Kildishev, T. D. Sands and A. Boltasseva, Opt. Mater. Express **2** (4), 478-489 (2012).
118. G. V. Naik, J. Kim and A. Boltasseva, Opt. Mater. Express **1** (6), 1090-1099 (2011).
119. Y. Konishi, I. Tanabe and T. Tatsuma, Chemical Communications **49** (6), 606-608 (2013).
120. F. B. Atar, E. Battal, L. E. Aygun, B. Daglar, M. Bayindir and A. K. Okyay, Opt. Express **21** (6), 7196-7201 (2013).
121. C. Binns, Surface Science Reports **44** (1–2), 1-49 (2001).
122. R. E. Palmer, S. Pratontep and H. G. Boyen, Nat Mater **2** (7), 443-448 (2003).
123. K. Wegner, P. Piseri, H. V. Tafreshi and P. Milani, Journal of Physics D: Applied Physics **39** (22), R439 (2006).
124. A. I. Ayesh, N. Qamhieh, H. Ghamlouche, S. Thaker and M. El-Shaer, Journal of Applied Physics **107** (3), 034317 (2010).
125. A. Marek, J. Valter, S. Kadlec and J. Vyskočil, Surface and Coatings Technology **205, Supplement 2** (0), S573-S576 (2011).
126. P. Thangadurai, I. Zergioti, S. Saranu, C. Chandrinou, Z. Yang, D. Tsoukalas, A. Kean and N. Boukos, Applied Surface Science **257** (12), 5366-5369 (2011).